Comparison of versions 6 and 7 3-hourly TRMM multi-satellite precipitation analysis (TMPA) research products

CrossMark

Zhong Liu *

Center for Spatial Information Science and Systems (CSISS), George Mason University, Fairfax, VA 22030, USA
Goddard Earth Sciences Data and Information Services Center (GES DISC), NASA Goddard Space Flight Center, Code 610.2, Greenbelt, MD 20771, USA

ABSTRACT

This paper examines differences between Version 6 (V6) and Version 7 (V7) 3-hourly TRMM (Tropical Rainfall Measuring Mission) Multi-Satellite Precipitation Analysis (TMPA 3B42) research products in JJA (June, July and August) and DJF (December, January and February) over a 13-year period from 1998 to 2010 on a global scale. Different surface types and rain regimes are considered in the comparison. The study finds that more rain events are found in V7 than those in V6 in both JJA and DJF, especially over oceans. Overall, both versions show a good agreement in moderate and heavy rain regimes. High Pearson's correlation coefficients are found in tropical rain band regions. Histograms of both versions are very similar; however higher frequencies of rain events are found in V7 in light rain regime, especially over oceans, than those in V6. For light rain, rainfall estimates in V6 are less than those in V7 over land and oceans in both seasons. For moderate rain, rainfall estimates in V6 are larger than those in V7 over land in most years. Over oceans, it is a mixed situation in which V6 > V7 for some years and V6 < V7 for the other years. For heavy rain, rainfall estimates in V6 are larger than those in V7 throughout all JJA and DJF seasons for both land and oceans, which is also shown in a case study. Large variance in the individual differences is found in light rain and less in heavy rain. No apparent trends are observed. For light rain, all statistics support that there is an uncertainty issue in both versions.

© 2015 The Author. Published by Elsevier B.V. This is an open access article under the CC BY-NC-ND license (http://creativecommons.org/licenses/by-nc-nd/4.0/).

1. Introduction

Accurate measurement and prediction of precipitation can greatly help hazard preparedness and mitigation efforts. However, precipitation is notoriously difficult to measure and predict, especially in remote and data sparse regions. In the past two decades, satellite-derived products provide a cost-effective way to measure precipitation from space and fill in data gaps in data sparse regions (Adler et al., 2003; Huffman et al., 1995, 2001, 2007, 2010; Joyce et al., 2004; Mahrooghy et al., 2012; Hong et al., 2007; Sorooshian et al., 2000; Behrangi et al., 2009; Aonashi et al., 2009). In recent years, near-global precipitation products have been developed with algorithms that utilize multi-satellites and multi-sensors that consist of microwave sensors, geostationary infrared sensors, ground radar network and gauges for bias correction (i.e., Huffman et al., 1995, 2001, 2007, 2010; Joyce et al., 2004; Mahrooghy et al., 2012; Hong et al., 2007; Sorooshian et al., 2000; Behrangi et al., 2009; Aonashi et al., 2009) and are widely used in

hydrometeorological research and applications. An example is the 3-hourly TRMM (Tropical Rainfall Measuring Mission) Multi-Satellite Precipitation Analysis (TMPA) that consists of two products: near-real-time (3B42RT) and research-grade (3B42). The former provides quick, less accurate estimates suitable for monitoring activities; the latter provides more accurate estimates more suitable for research. As the TMPA algorithm is improved and newer version is released, changes in product characteristics need to be well understood and documented in order for users to compare results from the previous version or make adjustments or changes to their applications and research.

In this study, differences between Version 6 (V6) and Version 7 (V7) 3-hourly TMPA research products (3B42) are investigated on a global scale over a 13-year period from 1998 to 2010. The NASA Goddard Earth Sciences Data and Information Services Center (GES DISC) is home to the NASA-JAXA (the Japan Aerospace Exploration Agency) Tropical Rainfall Measuring Mission (TRMM, TRMM special issue 2000) data archive (Liu et al., 2012). Both products are archived and distributed at the GES DISC (Liu et al., 2012). Documenting and providing such information are an important part of the GES DISC user services, benefiting not only the precipitation community, but also other communities as well. There have been several assessment studies with

* Center for Spatial Information Science and Systems (CSISS), George Mason University, Fairfax, VA 22030, USA. Tel.: +1 301 614 5764; fax: +1 301 614 5268.
E-mail address: Zhong.Liu@nasa.gov.

Table 1
List of V6 and V7 TMPA product information.

Version	Temporal resolution	Spatial resolution	Date range	Parameters
6	3-hourly	0.25×0.25 degree	January 1, 1998–June 30, 2011	• Precipitation • Random Error
7	3-hourly	0.25×0.25 degree	January 1, 1998–present	• Precipitation • Random Error • Satellite Source • HQ Precipitation • IR Precipitation • Satellite Observation Time

data from gauges, radars and ocean buoys at regional levels such as the United States, the People's Republic of China, India, the northern Peruvian Andes, tropical oceans (Huffman et al., 2012; Zulkafli et al., 2014; Prakash et al., 2013, 2014; Qiao et al., 2014; Yong et al., 2014a, 2014b; Chen et al., 2013a, 2013b) and results show various degrees of improvement in V7; however, direct comparison between V6 and V7 on a global scale in different rain regimes and over different surface types has not been reported to the author's knowledge and therefore this study is warranted. The article is organized as follows: Section 2 describes the TMPA products, the algorithm changes and statistical methods, Section 3 the results, and Section 4 the conclusions and discussion.

2. Data and methods

The purpose of the TMPA algorithm is to produce TRMM merged high quality (HQ) microwave/infrared (IR) precipitation and root-mean-square (RMS) precipitation-error estimates (Huffman et al., 2007, 2010; Huffman and Bolvin, 2013) in the following stages: (1) The microwave precipitation estimates are calibrated and combined, (2) The infrared precipitation estimates are created using the calibrated microwave precipitation, (3) The HQ and IR estimates are combined, and (4) Rescaling to monthly data is applied. In May 2012, V7 was implemented (Huffman and Bolvin, 2013) to replaceV6. Major changes are summarized by Huffman and Bolvin (2013):

- Additional satellites have been added, including the early parts of the Microwave Humidity Sounder (MHS) record, the entire operational Special Sensor Microwave Imager-Sounder (SSMIS) record, and slots for future satellites.
- A new National Climate Data Center (NCDC) IR brightness temperature dataset (GridSat-B1) for the period before the start of the Climate

Prediction Center (CPC) 4-km Merged Global IR Dataset (i.e., January 1998 – February 2000) has been included. Unlike the old Global Precipitation Climatology Project (GPCP) histograms used in V6, the GridSat-B1 features spatial resolution finer than the TMPA 0.25 grid and full coverage of the TMPA domain.
- Uniformly reprocessed input data using current algorithms, most notably for Advanced Microwave Sounding Unit (AMSU) and MHS, but also including TRMM Combined Instrument (TCI), TRMM Microwave Imager (TMI), the Advanced Microwave Scanning Radiometer for Earth Observing System (AMSR-E), and the Special Sensor Microwave Imager (SSMI).
- Use of a single, uniformly processed surface precipitation gauge analysis using current algorithms as computed by the Global Precipitation Climatology Centre (GPCC).
- Use of a latitude-band calibration scheme for all satellites.
- Additional output fields in the data files, including sensor-specific source and overpass time.

Both V6 and V7 products listed in Table 1 are used in this study. They are archived and distributed at the NASA GES DISC. Both versions were downloaded from the GES DISC data search and ordering system, Mirador (http://mirador.gsfc.nasa.gov/). Data services, i.e., format conversion, subsetting, are available to facilitate data access (Liu et al., 2012). There have been few product issues (Huffman and Bolvin, 2013). All the products used in this study are the latest.

To facilitate precipitation product intercomparison, the GES DISC has developed prototypes in the TRMM Online Visualization and Analysis System (TOVAS) (Liu et al., 2007, 2009, 2014). TOVAS (http://disc.sci.gsfc.nasa.gov/precipitation/tovas) is a member of the Geospatial Interactive Online Visualization ANd aNalysis Infrastructure (Giovanni, http://giovanni.gsfc.nasa.gov) (Liu et al., 2007; Acker and Leptoukh, 2007; Berrick et al., 2009). Giovanni is a Web-based application that

Table 2
Ratio of total grid count between V6 and V7 in the Northern Hemisphere and non-rainy (zero rain rate) grid count frequency (divided by the total grids) for JJA.

Year	Ratio of total grid count (V6/V7)	Non-rainy grid count (frequency)			
		Land		Ocean	
		V6	V7	V6	V7
1998	84%	0.92	0.91	0.88	0.83
1999	87%	0.92	0.91	0.89	0.82
2000	100%	0.94	0.91	0.90	0.83
2001	100%	0.93	0.92	0.91	0.86
2002	100%	0.93	0.92	0.91	0.86
2003	100%	0.93	0.92	0.92	0.86
2004	100%	0.93	0.92	0.91	0.86
2005	100%	0.93	0.91	0.91	0.86
2006	100%	0.92	0.91	0.91	0.86
2007	100%	0.92	0.91	0.90	0.87
2008	100%	0.92	0.91	0.90	0.86
2009	100%	0.92	0.92	0.90	0.87
2010	100%	0.91	0.92	0.89	0.86

Table 3
Ratio of total grid count between V6 and V7 in the Southern Hemisphere and non-rainy (zero rain rate) grid count frequency (divided by the total grids) for DJF.

| Year	Ratio of total grid count (V6/V7)	Non-rainy grid count (frequency)			
		Land		Ocean	
		V6	V7	V6	V7
1998	87%	0.89	0.88	0.91	0.84
1999	90%	0.88	0.87	0.91	0.85
2000	100%	0.88	0.87	0.92	0.88
2001	100%	0.89	0.88	0.92	0.88
2002	100%	0.89	0.88	0.92	0.88
2003	100%	0.88	0.88	0.93	0.88
2004	100%	0.87	0.89	0.92	0.88
2005	100%	0.88	0.87	0.92	0.88
2006	100%	0.88	0.87	0.92	0.89
2007	100%	0.88	0.87	0.91	0.89
2008	100%	0.87	0.87	0.91	0.89
2009	100%	0.87	0.88	0.90	0.90
2010	100%	0.85	0.87	0.90	0.89
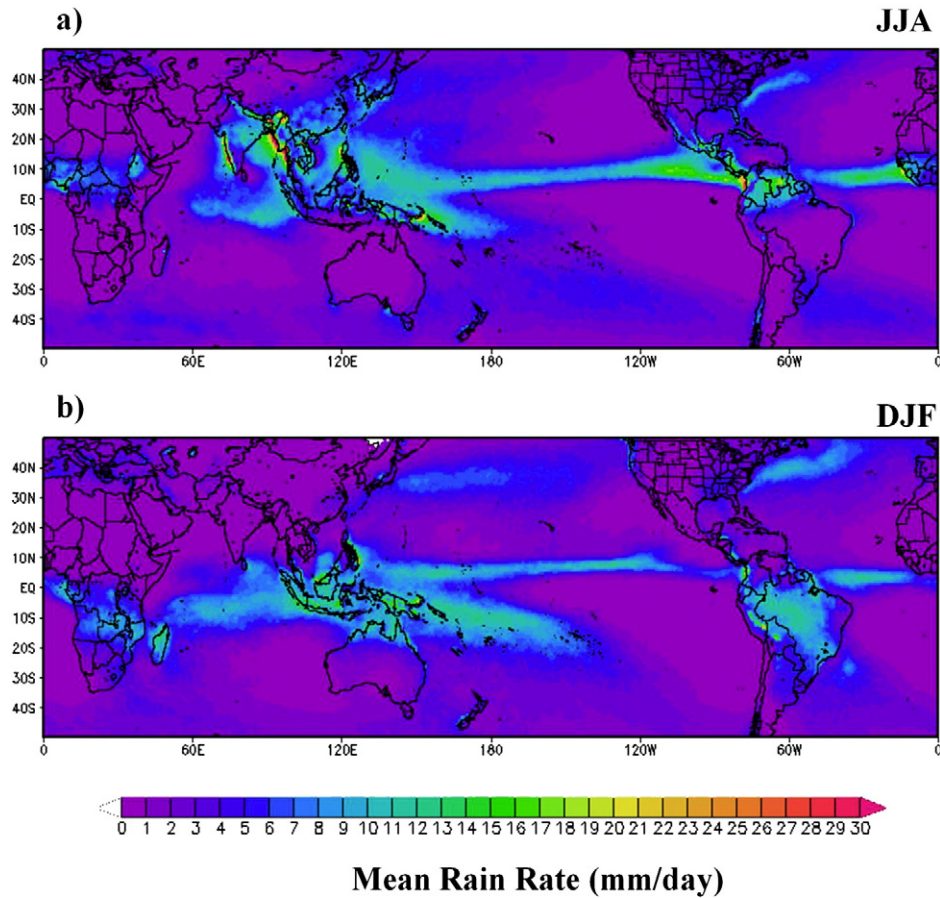
Fig. 1. Mean seasonal rain rate (in mm/day) averaged between 1998 and 2010: JJA (top) and DJF (bottom).

provides a simple and intuitive way to visualize, analyze, and access vast amounts of Earth science remote sensing data without having to download the data (Acker and Leptoukh, 2007; Berrick et al., 2009; Liu et al., 2014). Basic and customized comparison (i.e., scatter plot, Pearson's correlation, time series, etc.) between the TMPA near-real-time and research products as well as their preceding versions can be done via either TOVAS (Liu et al., 2014) or offline analysis using customized data from TOVAS. Statistical methods (http://www.cawcr.gov.au/projects/verification/) used in the International Precipitation Working Group (IPWG) validation sites are being added in TOVAS.

In this study, two major rainy seasons, the boreal summer (June, July and August, JJA hereafter) and the austral summer (December, January and February, DJF hereafter) are considered because precipitation reaches the maximum amount in these seasons in the Northern and Southern Hemispheres, respectively. Furthermore, land and oceans are separately divided in computing statistics in order to better observe product error components. Different rain regimes are considered as well.

Mean difference (MD), mean absolute difference (MAD) and root mean square difference (RMSD) (i.e., Ebert, 2007) are used to measure differences between the two products. If observational data are used for evaluation, MD is also equivalent to bias (Ebert, 2007). For MAD, an equal weight is given to each difference. By contrast, a relatively higher weight is given to larger differences because they are squared before averaging. In general, RMSD is larger than MAD and both of them can be used together to examine the variance in differences: the larger the difference between MAD and RMSD, the larger the variance in the individual differences in the data set. When MAD is equal to RMSD or

the ratio between MAD and RMSD is equal to 1, there is no variation in differences. In general, the smaller MD, MAD, and RMSD are, the smaller the difference is between both products. The equations of MD, MAD and RMSD (Ebert, 2007) are written as:

$$MD = \frac{1}{N} \sum_{i=1}^{N} (Y_i - O_i) \tag{1}$$

$$MAD = \frac{1}{N} \sum_{i=1}^{N} |Y_i - O_i| \tag{2}$$

$$RMSD = \sqrt{\frac{1}{N} \sum_{i=1}^{N} (Y_i - O_i)^2} \tag{3}$$

where, Y_i is the estimated value of 3B42 V6 and O_i 3B42 V7 at grid box i, and N is the size of the sample.

The data processing is done as follows. First, MD, MAD, and RMSD for the two products are computed for each season and averaged for each season over the period 1998 to 2010 at each grid point for the entire data domain (50°N–50°S). These seasonal means are then averaged and the final result is a mean seasonal map. For time series, an areal average is computed for each statistical parameter for each season for the Northern Hemisphere (JJA) and the Southern Hemisphere (DJF) separately and a time series table is generated with these averages.

Direct comparison of MD, MAD and RMSD can be an issue because rain rate can vary from one grid point to another. Relative (to the mean 3B42 rain rate) MD and MAD in percentage are used, instead. In

addition, the ratio between MAD and RMSD (M/R ratio hereafter) is used to measure the variance in the individual differences. As mentioned earlier, when the ratio is equal to 1, there is no variation in the individual differences. On the other hand, the smaller the ratio is, the larger the variance in the individual differences.

To investigate the inter-annual variations of MD, MAD and RMSD under different rain regimes, three groups are defined (http://www. metoffice.gov.uk/media/pdf/4/1/No._03_-_Water_in_the_Atmosphere. pdf), light rain (rain rate ≤ 2.5 mm/h), moderate rain (2.5 mm/h < rain rate ≤ 10 mm/h) and heavy rain (10 mm/h < rain rate ≤ 50 mm/h). For rain rate that is greater than 50 mm/hr, the sample sizes are too small and in some years no data are available; therefore such rain is not included in this study. Note that the American Meteorological Society has slightly different thresholds for rain classifications (http://glossary. ametsoc.org/wiki/Rain); but nonetheless, the purpose here is to investigate statistical variations in different rain regimes.

Missing data are common in remote sensing products due to various reasons, which can have an impact on computing statistics for comparison. Tables 2 and 3 list ratios of total grid count between V6 and V7 for the Northern Hemisphere in JJA and the Southern Hemisphere in DJF from 1998 to 2010, respectively. It is seen that more data were added in V7 in 1998 and 1999 in both JJA and DJF due to, as mentioned earlier in Section 2, a new NCDC IR brightness temperature dataset (GridSat-B1) that was included in this period. Throughout the rest of the study period, the ratio between V6 and V7 has remained near 100%, which means the data counts for both versions are nearly equal. Both tables list the frequencies (divided to the total grid count) for non-rainy (zero rain rate) grid count over land and oceans. It is shown that V6, in general, has more non-rainy grids or higher frequencies of no-rain events, especially over oceans than those in V7 in both JJA and DJF

during the period from 2000 to 2010. Over land, V6 has slightly more non-rainy grids than in V7 and in some years V7 has more than V6. In 1998 and 1999, the frequencies of no-rain events for V6 are higher than those in V7 in Tables 2 and 3, but when considering the missing data in V6 during the two year period, the total non-rainy grids in V6 each year are slightly less than those in V7.

3. Results

3.1. Basic characteristics

Fig. 1 is the near-global (50°N–50°S) mean seasonal V7 rainfall estimates for JJA and DJF, averaged between 1998 and 2010, respectively. In JJA and DJF, it is seen that rainfall mainly concentrates in the tropics. High rain rate regions (Fig. 1a) in JJA are found in the Inter-Tropical Convergence Zone (ITCZ) and near coastal mountainous regions such as the Western Ghats in western Indian, Myanmar (Burma), where orography lifts the incoming moist oceanic airflow and enhances rainfall. In DJF (Fig. 1b), overall, rain rate is not as high as in JJA and high rain rate regions are primarily confined to the tropics. Large standard deviations are also found in the high rain rate regions as well (not shown), especially in the western Pacific warm pool in DJF, indicating a strong inter-annual variation in rainfall amount. This variation is contributed by many factors, such as, the El Niño Southern Oscillation (ENSO), the Pacific Decadal Oscillation (PDO), tropical cyclones, the Madden–Julian oscillation (MJO), etc. Detailed discussion is beyond the scope of this study. Although large standard deviations are found in the tropics, their relative (with respect to their means) values are small compared to the other parts of the world (Fig. 2) in both JJA and DJF. By contrast, small standard deviations are
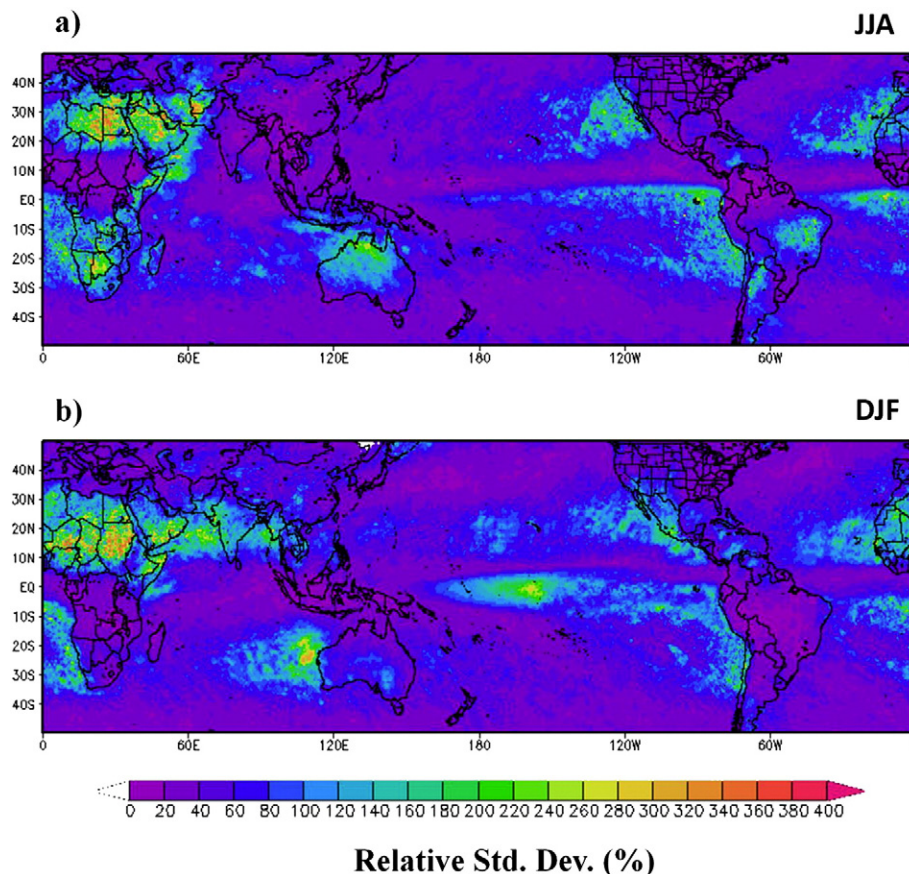

Fig. 2. Mean relative (to the mean in Fig. 1) seasonal standard deviation (in %) averaged between 1998 and 2010: JJA (a) and DJF (b).
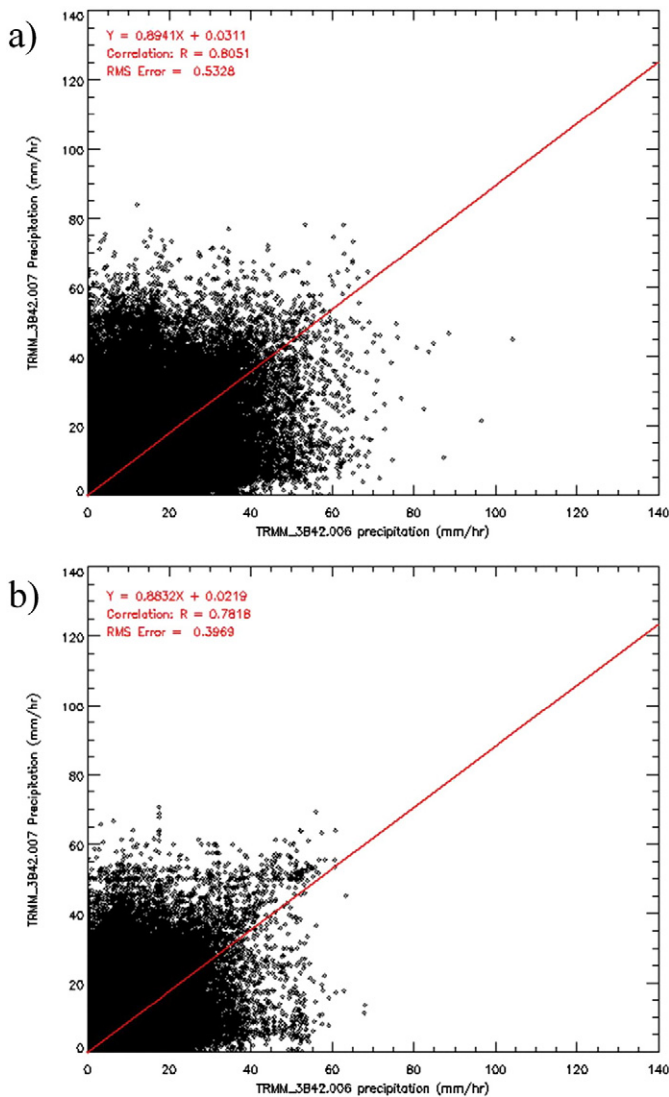
Fig. 3. Scatter plots between V6 and V7 in 2003: (a) Northern Hemisphere (JJA); (b) Southern Hemisphere (DJF). The redline is the linear fit line.

found in light rain regions, but their relative values are much larger than those in high rain rate regions and in some places, they exceed well over 100% of their means (Fig. 2).

Fig. 3 contains two typical scatterplots for JJA in the Northern Hemisphere (Fig. 3a) and DJF in the Southern Hemisphere (Fig. 3b) in 2003. As shown in Fig. 1, rain rate distribution and magnitudes can vary with season; therefore only the Northern Hemisphere is included in JJA and the Southern Hemisphere in DJF. Fig. 3 shows that more high rain rate points in JJA than those in DJF, which is consistent with the finding in Fig. 1. There are some false alarm samples along both V6 and V7 axes (Fig. 3), mainly in the light to moderate rain ranges, where no rain is found in V7 and rain found in V6, or vice versa. In a study by Huffman et al. (2007, 2010), it is concluded that the TMPA has lower skill in detecting light to moderate rain events. The linear fit lines that are below the 1:1 line in both JJA and DJF share some common characteristics: a) The V7 intercept value is above zero, indicating that a systematic difference (V6 < V7) in light rain events and b) The slope that is less than one suggests the opposite systematic difference (V6 > V7) in higher rain rates. More details are presented Section 3.2 and a case study.

Fig. 4 consists of two mean Pearson's correlation coefficient maps derived from the JJA and DJF seasons between 1998 and 2010,

respectively. Overall, high positive correlation coefficients dominate in high rain rate regions in both JJA and DJF (Fig. 4) as well as in other rainy regions. Correlation coefficients decrease outside the belt between 40°N–40°S (Fig. 4). Few negative correlation coefficients are scattered in various places such as Europe. Negative correlation coefficients are also found in the belts between 40°S–50°S in both JJA and DJF. These negative points perhaps are related to the uncertainty in light precipitation estimation as mentioned earlier. In short, despite the version change, rain rates in major rainy regions maintain a good linear relationship in JJA and DJF between 1998 and 2010.

Figs. 5 and 6 are the histograms of rain rate frequencies and their inter-annual variations over land and oceans for the Northern Hemisphere (JJA) and the Southern Hemisphere (DJF) between 1998 and 2010. The distribution patterns of both versions are very similar with highest frequencies in the light rain regime; however the inter-annual variations between the two versions are quite different, although in the same version, the inter-annual variations in both JJA and DJF are similar. The highest frequency is found in the zero rain rate (Tables 2 and 3) in each version, followed by the bins of (0.01–1.0) mm/hr and (1.0–5.0) mm/hr. In Figs. 5 and 6, it is seen that the extra non-rainy grids in V7 in Tables 2 and 3 go to the bin of (0.01–1.0) mm/hr over land and oceans in both JJA and DJF. This increase in grid count is more visible over oceans, as suggested in Tables 2 and 3 where the difference in non-rainy grid count is larger over oceans than over land.

3.2. Relative mean difference (RMD), relative mean absolute difference (RMAD) and ratio (M/R) between MAD and root mean square difference (RMSD)

Fig. 7 shows RMD (relative to the mean V7 rain rate) for JJA and DJF, respectively. In general, negative RMD (V6 < V7) dominates over oceans and positive RMD (V6 > V7) over land. Large negative RMD values over oceans are found in light rain regions (Fig. 7). By contrast, small negative RMD values are found in the tropical rain band regions (Fig. 7). In JJA, negative RMD values are found in most low latitude regions. In particular, high negative RMD values are found in the tropical latitudes, such as in the coastal areas of Myanmar (Burma), the southern Mexico, Columbia, etc. In JJA, positive RMD values are found in high latitudes, such as the belts outside 40° N and 40° S latitudes, respectively. Some large positive RMD values are found over the east equatorial Pacific Ocean in JJA. In DJF, negative RMD values dominate, similar to those in JJA; however, the magnitudes are less than those in JJA. In some regions, the sign of RMD values is reversed from positive in JJA to negative, such as the belt outside 40° S. Similar to that in JJA, the North Pacific maintains positive in both seasons.

Unlike RMD, RMAD for JJA and DJF in Fig. 8 shows more consistent patterns in both seasons, namely, high MAD values are found in high rain rate regions (not shown) and low in light rain regions. Compared to their means, RMAD values are small (Fig. 8) in high rain rate regions and large in light rain regions. For example, in JJA, high RMAD values are found along the coastlines of west India, Myanmar, etc.

As mentioned in Section 2, the ratio (M/R) between MAD and RMSD represents the variance in the individual differences: the larger the ratio, the smaller the variance. When the ratio is equal to 1, there is no variance in the individual differences. Fig. 9 shows the M/R ratios in which the patterns are very similar to those in Fig. 8, small variance in differences is found in high rain rate regions and large variance in light rain regions.

Tables 4 and 5 show the inter-annual variation of RMD over land and oceans for rain regimes from light to heavy rain in JJA and DJF, respectively. For light rain, RMD values are all negative in both seasons between 1998 and 2010, suggesting light rain estimates in V6 are smaller than those in V7, which is consistent with the finding from the scatter plots in Fig. 3. For moderate rain, positive RMD values
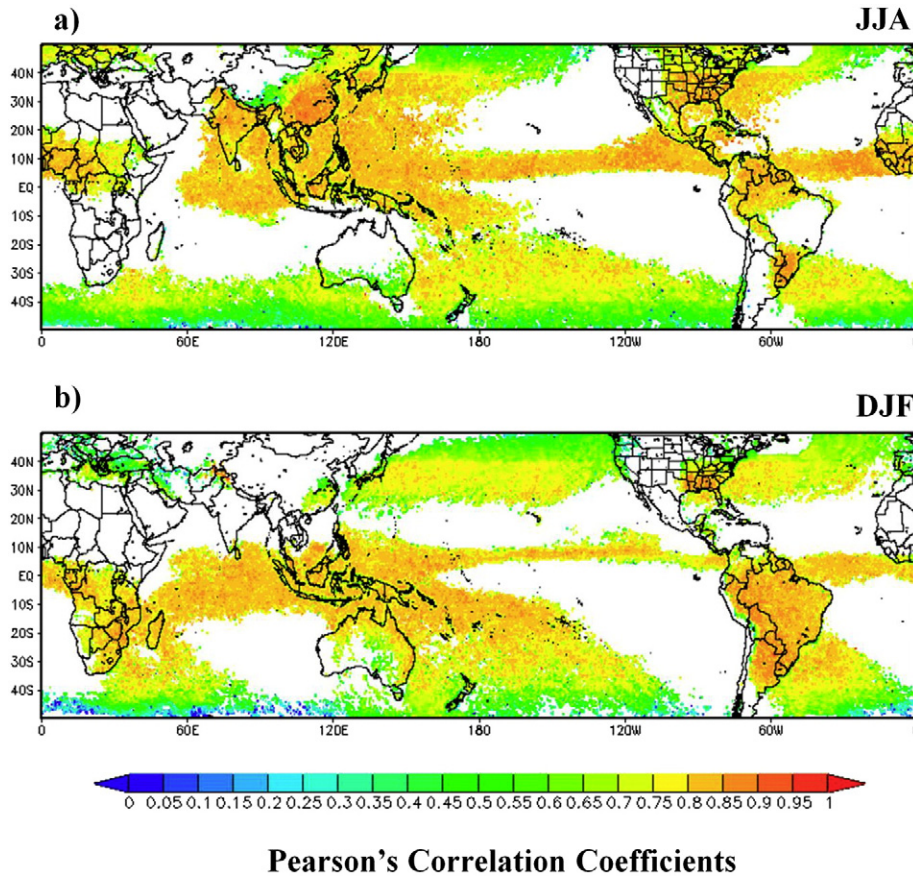
Pearson's Correlation Coefficients

Fig. 4. Mean seasonal Pearson correlation coefficients between 1998 and 2010 for JJA (a) and DJF (b).
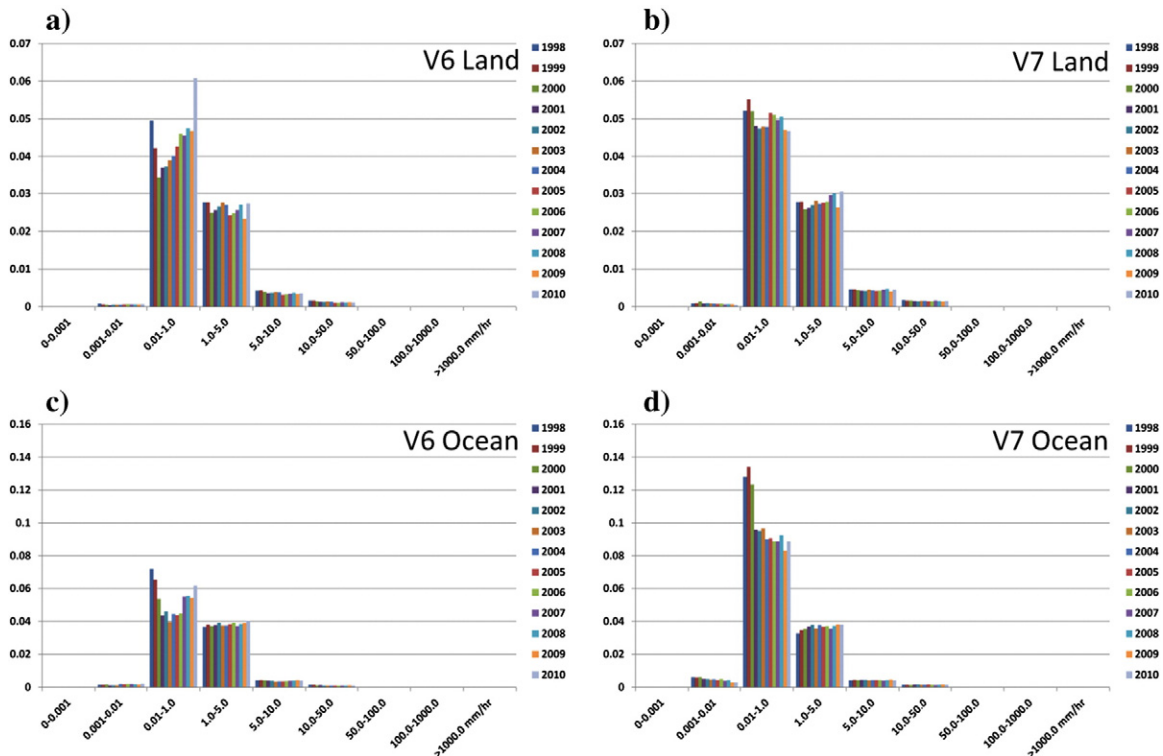

Fig. 5. Histograms of rain rate frequency for the Northern Hemisphere in JJA: a) V6 land; b) V7 land; c) V6 ocean and d) V7 ocean. The frequencies for zero rain rate are listed in Table 2.
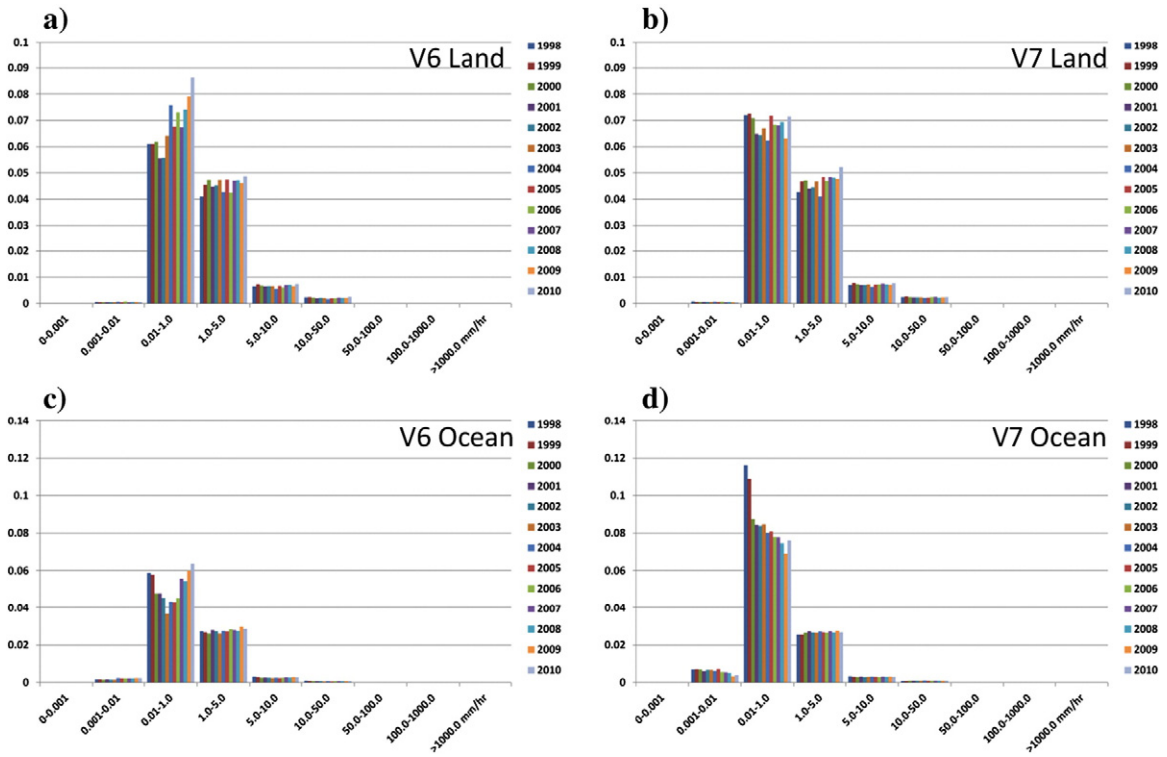
Fig. 6. Histograms of rain rate frequency for the Southern Hemisphere in DJF between 1998 and 2010: a) V6 land; b) V7 land; c) V6 ocean and d) V7 ocean. The frequencies for zero rain rate are listed in Table 3.
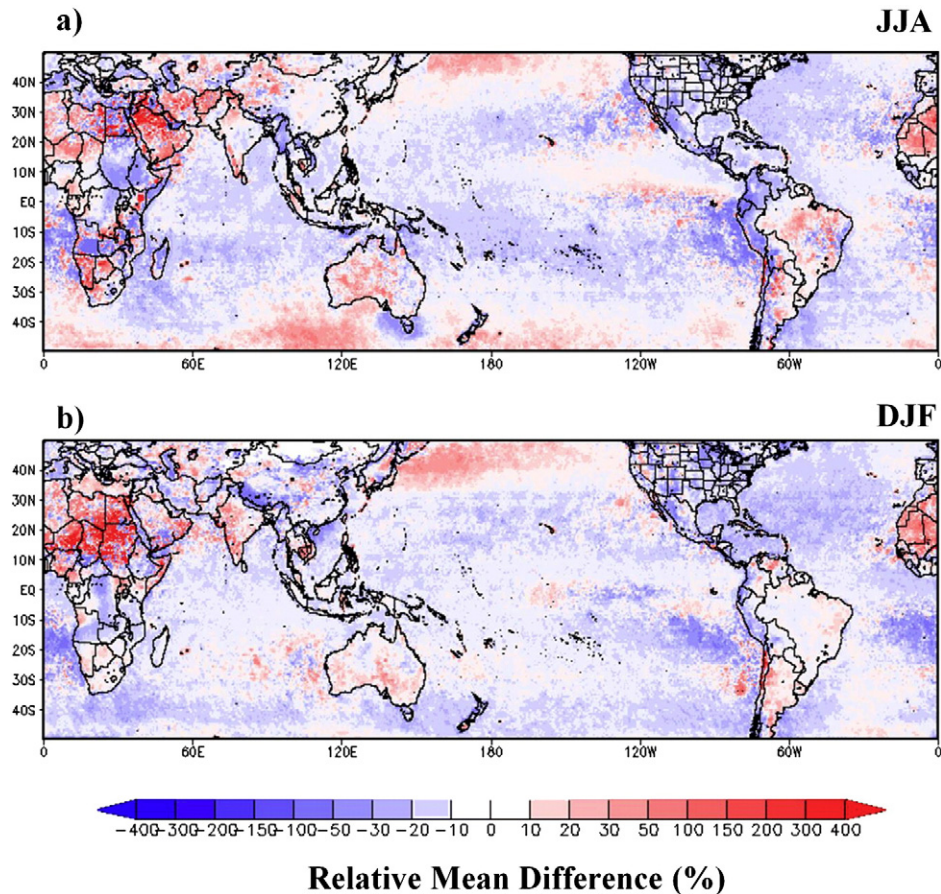

Fig. 7. Mean relative (with respect to the mean) MD in percentage between 1998 and 2010 for: a) JJA and b) DJF.
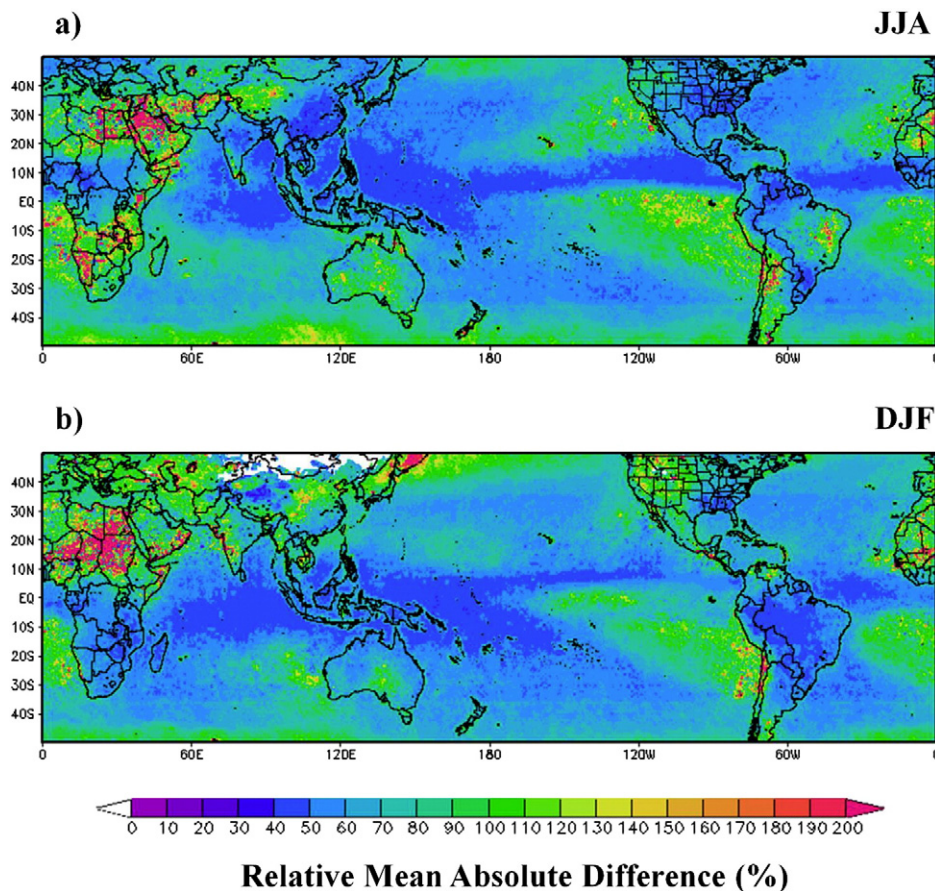
Fig. 8. Relative MAD in percentage between 1998 and 2010 for: a) JJA and b) DJF.

dominate over land and there is only one season when RMD values are negative. Over oceans, negative RMD values are found in nearly half of the years between 1998 to 2010. For heavy rain, there is no negative RMD and all RMD values are positive, suggesting V6 rain rates are higher than those in V7. No apparent trends are observed over both land and oceans.

Fig. 10 shows V6 and V7 rainfall estimates for Typhoon Matsa at 00Z on August 5, 2005. Matsa dumped heavy rain when it passed Taiwan and made a landfall in Zhejiang province in the People's Republic of China, causing 25 direct fatalities and $18 billion in damage (http://en. wikipedia.org/wiki/Typhoon_Matsa). Fig. 10a and b show the V6 and V7 rainfall estimates, respectively, when Matsa was about to make a landfall in Zhejiang province. Their difference is shown in Fig. 10c. Overall, the rainfall patterns of V6 and V7 are quite similar such as that the heaviest rain centers are both located off the coast of Zhejiang province. However, the rain rate estimates are quite different, as seen in Fig. 10c where V6 clearly has higher estimates near the typhoon center than those in V7 (Fig. 10c). Again the scatter plot in Fig. 8d is similar to those in Fig. 3, namely, V6 < V7 in light rain and V6 > V7 in heavy rain.

Tables 6 and 7 contain the inter-annual variations of RMAD and M/R ratios for moderate and heavy rain regimes. For moderate rain, the RMAD values over land in JJA are slightly larger than those over oceans; but in DJF, the opposite is found. For heavy rain, the RMAD values over oceans are in general larger than those over land in both JJA and DJF. Compared to the M/R ratios in moderate rain, the M/R ratios in heavy rain are much higher, suggesting the variance in the individual differences are smaller in heavy rain. In Tables 6 and 7, there is no apparent trend in all RMAD and M/R ratios.

4. Conclusions and discussion

This paper examines differences between V6 and V7 TMPA 3B42 research products in JJA and DJF, respectively, in JJA and DJF in different rain regimes over different surface types on a global scale to better understand the changes in product characteristics due to the version change. The results show that more rain events are found in V7 than those in V6 in both JJA and DJF, especially over oceans, except in 1998 and 1999 due to missing data in V6. Large values of relative standard deviation are found in light rain regions over land and oceans; by contrast, small values are found in tropical high rain rate regions. Scatter plots show the uncertainty in light rain regime. The linear fit line suggests two systematic differences between V6 and V7: V6 < V7 for light rain and V6 > V7 for heavy rain. High Pearson's correlation coefficients are found in the tropical rain band regions, suggesting high consistency in both versions. Histograms of both versions are very similar; however higher frequencies for V7 are found in the light rain regime than those in V6, especially over oceans. Statistics for different rain regimes reveal more details on the systematic differences. For light rain, rainfall estimates in V6 are less than those in V7 over land and oceans in both seasons. For moderate rain, rainfall estimates in V6 are larger than those in V7 over land in most years. Over oceans, it is V6 > V7 in some years and the opposite for the other years. For heavy rain, rainfall estimates in V6 are larger than those in V7 in both JJA and DJF throughout the entire period (1998–2010), which is shown in a case study as well. Large variance in differences is associated with rain regimes and increases with rain rate. There is no apparent trend in the 13 year period (1998–2010).

Overall, both V6 and V7 show a good agreement in moderate and heavy rain regimes; however, systematic differences do exist and are
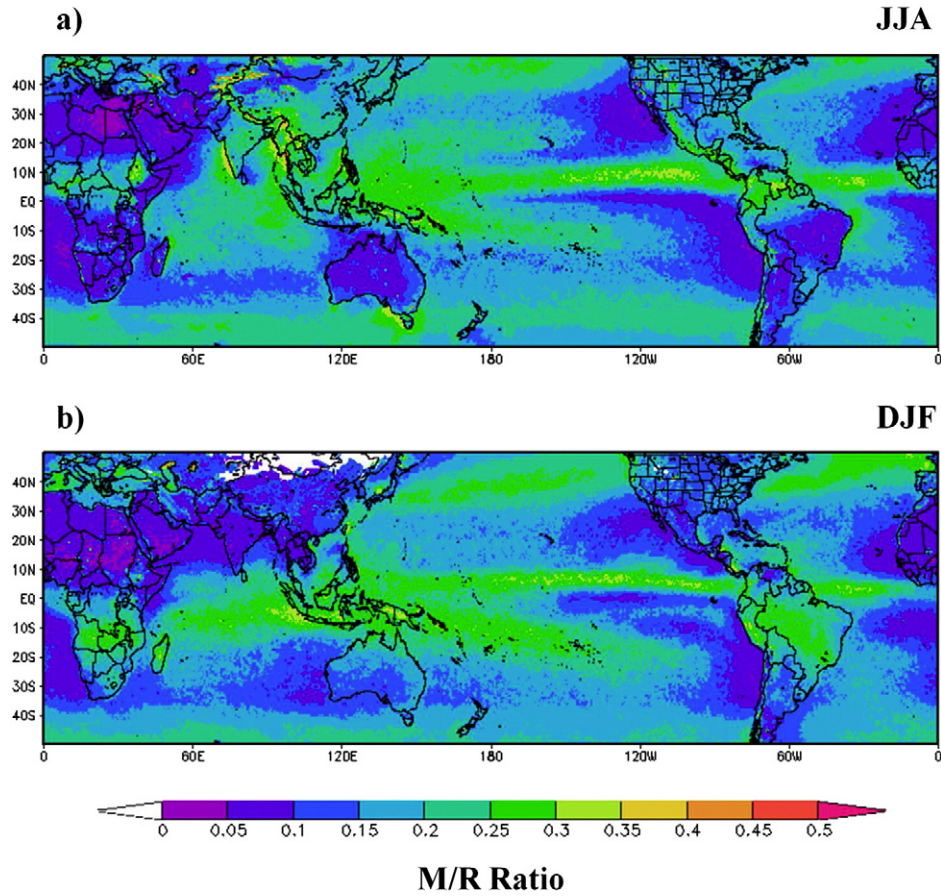
a)   JJA

b)   DJF

M/R Ratio

Fig. 9. M/R ratio between MAD and RMSD for: a) JJA and b) DJF.

characterized by V6 < V7 for light rain and V6 > V7 for heavy rain. For light rain, all statistics support that there is an uncertainty issue in both versions.

Results from previous studies (Huffman et al., 2012; Zulkafli et al., 2014; Prakash et al., 2013, 2014; Qiao et al., 2014; Yong et al., 2014a, 2014b; Chen et al., 2013a, 2013b) mainly focused on product improvement with direct comparison between TMPA and ground observations (gauges, radars and buoys). For such reason, few results from previous results can be compared with those in this study. Nonetheless these studies do shed some light on the difference between V6 and V7. For example, all of the time series averaged over tropical oceans (Huffman et al., 2012; Prakash et al., 2013) and other oceans (Liu et al., 2014) show a "V" shape trough or "sag" (Huffman et al.,

2012) in V6 in the middle of the 13-year period as the result of deficient AMSU precipitation estimates in V6, which can also be seen in Tables 4 and 5 since the average rain rates in the time series are dominated by light rain events. Based on the histograms in Figs. 5 and 6, it seems more rain events in V7, especially over oceans, may be associated with the AMSU improvement. Huffman et al. (2012) explained the higher precipitation estimates (shown in the time series) in V7 had not been fully understood. Qiao et al. (2014) and Yong et al. (2014a, 2014b) report that all the TMPA products significantly underestimate high rain rates in their regions of interest. As we have seen here, in high rain rates, V6 > V7 and as the result of this, the underestimation issue may be getting worse in V7 in high rain rates.

Table 4
Mean seasonal average of V7 3B42 rain rate (mm/hr) and relative mean difference (RMD) with respect to the mean seasonal average for the Northern Hemisphere in JJA.

Year	Light Rain				Moderate Rain				Heavy Rain			
	land		ocean		land		ocean		land		ocean	
	Avg	RMD	AVG	RMD	Avg	RMD	Avg	RMD	Avg	RMD	Avg	RMD
1998	0.05	−57%	0.07	−21%	4.45	11%	4.20	16%	14.91	25%	14.37	31%
1999	0.04	−56%	0.07	−25%	4.44	12%	4.26	15%	14.89	25%	14.21	30%
2000	0.04	−36%	0.06	−20%	4.47	5%	4.25	4%	14.61	14%	13.84	13%
2001	0.04	−31%	0.06	−24%	4.33	2%	4.25	−1%	14.83	16%	14.10	11%
2002	0.05	−32%	0.07	−27%	4.32	8%	4.15	−3%	14.83	16%	14.42	13%
2003	0.05	−36%	0.06	−34%	4.34	7%	4.13	−2%	14.73	19%	14.47	15%
2004	0.05	−25%	0.06	−32%	4.38	3%	4.15	−8%	14.88	17%	14.18	6%
2005	0.04	−55%	0.06	−31%	4.30	−3%	4.14	−6%	15.10	18%	14.25	9%
2006	0.05	−50%	0.06	−30%	4.31	0%	4.13	1%	14.90	17%	14.11	11%
2007	0.05	−64%	0.07	−23%	4.29	3%	4.18	8%	14.99	22%	14.33	17%
2008	0.05	−60%	0.07	−31%	4.30	9%	4.22	7%	14.44	24%	13.74	15%
2009	0.04	−59%	0.07	−32%	4.34	12%	4.24	10%	14.69	30%	14.06	17%
2010	0.05	−54%	0.07	−29%	4.24	13%	4.15	16%	14.41	29%	13.61	20%

Table 5
Similar to Table 4, except for the Southern Hemisphere in DJF.

Year	Light Rain				Moderate Rain				Heavy Rain			
	land		ocean		land		ocean		land		ocean	
	Avg	RMD	Avg	RMD	Avg	RMD	Avg	RMD	Avg	RMD	Avg	RMD
1998	0.07	−48%	0.05	−26%	4.49	13%	4.16	10%	14.78	30%	14.10	29%
1999	0.07	−45%	0.05	−28%	4.55	9%	4.17	11%	14.75	24%	14.05	26%
2000	0.08	−18%	0.05	−25%	4.41	2%	4.10	−7%	14.87	14%	14.10	12%
2001	0.08	−17%	0.05	−20%	4.43	1%	4.10	−8%	14.79	12%	14.25	10%
2002	0.08	−24%	0.05	−28%	4.40	6%	4.08	−2%	15.07	20%	14.39	15%
2003	0.08	−23%	0.04	−46%	4.41	4%	4.06	−7%	15.14	22%	14.12	12%
2004	0.08	−10%	0.05	−30%	4.37	−2%	4.06	−10%	14.93	15%	14.32	7%
2005	0.08	−26%	0.05	−35%	4.41	6%	4.03	−3%	15.26	22%	13.97	13%
2006	0.08	−47%	0.05	−32%	4.38	2%	4.04	8%	15.20	24%	14.16	20%
2007	0.08	−32%	0.05	−22%	4.45	10%	4.07	5%	14.85	23%	14.03	18%
2008	0.08	−30%	0.05	−27%	4.44	13%	4.08	7%	14.46	26%	13.85	15%
2009	0.08	−32%	0.06	−22%	4.41	13%	4.14	17%	14.80	27%	13.71	18%
2010	0.09	−39%	0.06	−23%	4.50	16%	4.10	22%	14.48	30%	13.78	20%

It is extremely challenging to conduct accurate precipitation estimation and evaluation for improvement on a global scale due to the lack of observations and availability of data despite those observations sometimes are available. Due to the fact that only two parameters (Table 1), precipitation estimate and random error are available in V6, it is difficult to explain some of the differences found in this study. By contrast, in addition to the two parameters, V7 provides HQ precipitation and IR precipitation along with satellite observation time and satellite precipitation source information. Without these crucial parameters in V6, it is difficult to know exact information such as satellite source because a grid point can be either from HQ or IR precipitation even though the difference between their input Level-2 (orbital) products is known. Fortunately, these details are retained for further analysis during the GPM era (http://pmm.nasa.gov/GPM). Nonetheless, to further understand version
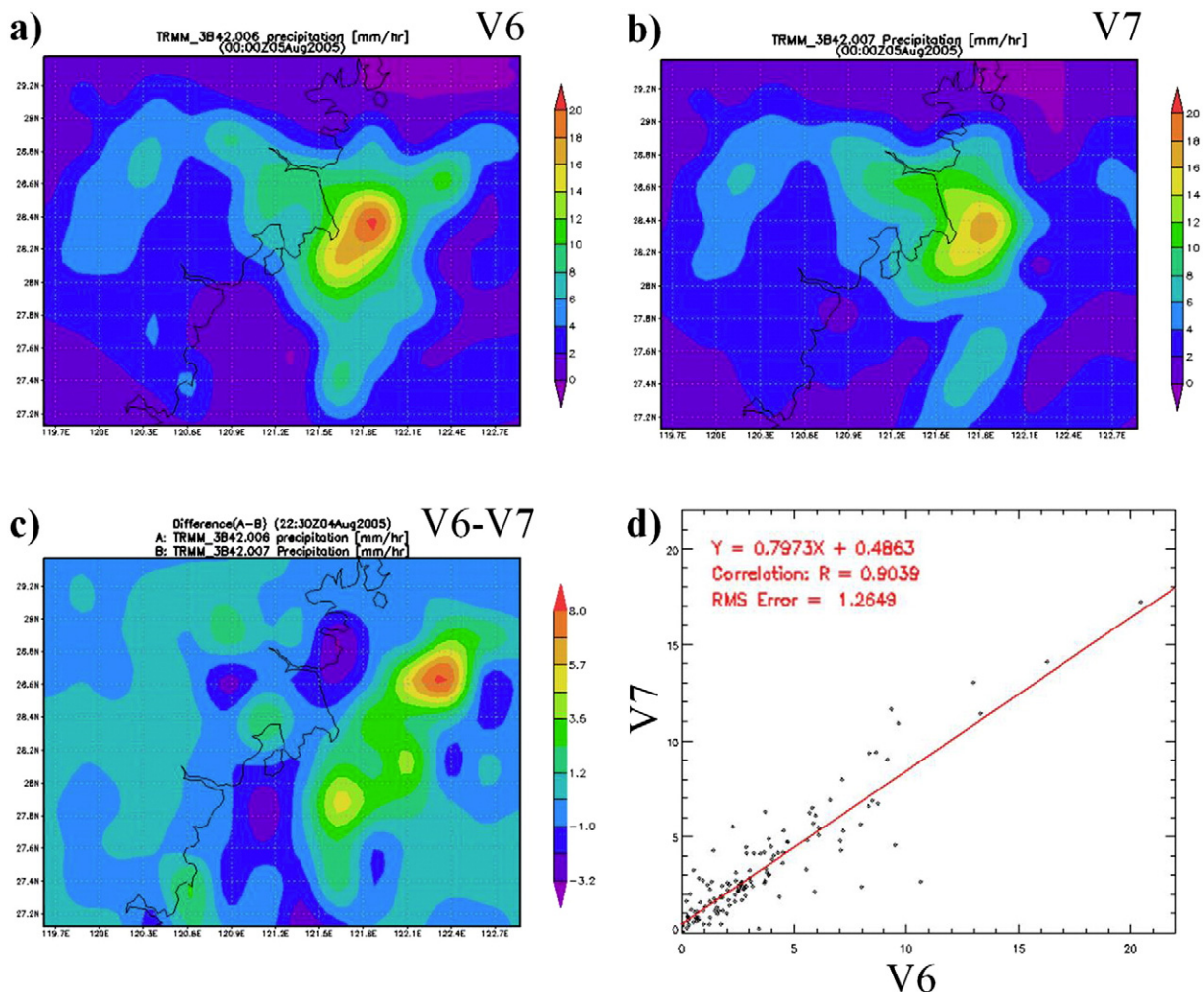

Fig. 10. Typhoon Matsa at 00Z on August 5, 2005: a) Version 6; b) Version 7; and c) their difference (V6-V7), and d) scatter plot (redline: the linear fit line).

Table 6
Relative mean absolute difference (RMAD) with respect to the mean seasonal average in Table 4 and M/R (MAD/RMSE) ratio for the Northern Hemisphere in JJA.

Year	Moderate Rain				Heavy Rain			
	land		ocean		land		ocean	
	RMAD	M/R	RMAD	M/R	RMAD	M/R	RMAD	M/R
1998	53%	0.81	48%	0.79	43%	0.91	45%	0.92
1999	50%	0.81	46%	0.79	41%	0.91	43%	0.93
2000	36%	0.77	30%	0.72	32%	0.90	33%	0.91
2001	37%	0.77	34%	0.72	33%	0.90	34%	0.90
2002	40%	0.77	41%	0.72	35%	0.90	40%	0.91
2003	42%	0.77	42%	0.74	38%	0.90	40%	0.91
2004	36%	0.76	39%	0.73	32%	0.90	36%	0.91
2005	46%	0.80	40%	0.72	36%	0.92	38%	0.91
2006	46%	0.79	41%	0.73	36%	0.91	38%	0.92
2007	51%	0.79	42%	0.73	39%	0.90	40%	0.91
2008	51%	0.79	44%	0.74	40%	0.90	41%	0.92
2009	50%	0.79	45%	0.75	43%	0.90	41%	0.91
2010	55%	0.80	49%	0.75	44%	0.91	43%	0.92

Table 7
Similar to Table 6, except for the Southern Hemisphere in DJF.

Year	Moderate Rain				Heavy Rain			
	land		ocean		land		ocean	
	RMAD	M/R	RMAD	M/R	RMAD	M/R	RMAD	M/R
1998	49%	0.78	47%	0.82	42%	0.91	42%	0.93
1999	45%	0.75	44%	0.81	38%	0.91	41%	0.93
2000	35%	0.74	37%	0.77	31%	0.88	34%	0.92
2001	34%	0.75	39%	0.75	30%	0.90	36%	0.92
2002	39%	0.75	44%	0.77	35%	0.89	40%	0.93
2003	39%	0.74	47%	0.77	36%	0.90	40%	0.93
2004	38%	0.75	44%	0.76	32%	0.91	38%	0.93
2005	39%	0.75	43%	0.77	36%	0.90	39%	0.93
2006	50%	0.77	47%	0.78	40%	0.89	44%	0.93
2007	42%	0.75	44%	0.77	37%	0.89	41%	0.92
2008	42%	0.75	45%	0.77	38%	0.89	41%	0.93
2009	46%	0.75	52%	0.79	40%	0.89	45%	0.93
2010	46%	0.75	53%	0.80	41%	0.89	44%	0.93

changes, the satellite source information along with Level-2 products is very important.

Acknowledgements

References

Acker, J.G., Leptoukh, G., 2007. Online analysis enhances use of NASA earth science data. Eos. Trans. Am. Geophys. Union 88 (2), 14–17.

Adler, R.F., Huffman, G.J., Chang, A., Ferraro, R., Xie, P., Janowiak, J., Rudolf, B., Schneider, U., Curtis, S., Bolvin, D., Gruber, A., Susskind, J., Arkin, P., Nelkin, E., 2003. The Version 2 Global Precipitation Climatology Project (GPCP) Monthly Precipitation Analysis (1979-Present). J. Hydrometeorol. 4, 1147–1167.

Aonashi, K., Awaka, J., Hirose, M., Kozu, T., Kubota, T., Liu, G., Shige, S., Kida, S., Seto, S., Takahashi, N., Takayabu, Y.N., 2009. GSMaP passive, microwave precipitation retrieval algorithm: Algorithm description and validation. J. Meteorol. Soc. Jpn. 87A, 119–136.

Behrangi, A., Hsu, K.-L., Imam, B., Sorooshian, S., Huffman, G.J., Kuligowski, R.J., 2009. PERSIANN-MSA: A Precipitation Estimation Method from Satellite-Based Multispectral Analysis. J. Hydrometeorol 10, 1414–1429. http://dx.doi.org/10.1175/2009JHM1139.1.

Berrick, S.W., Leptoukh, G., Farley, J.D., Rui, H., 2009. Giovanni: A Web service workflow-based data visualization and analysis system. IEEE Trans. Geosci. Remote Sens. 47 (1), 106–113.

Chen, S., Hong, Y., Gourley, J.J., Huffman, G.J., Tian, Y., Cao, Q., Yong, B., Kirstetter, P.E., Hu, J., Hardy, J., Li, Z., Khan, S.I., Xue, X., 2013a. Evaluation of the successive V6 and V7 TRMM multisatellite precipitation analysis over the Continental United States. Water Resour. Res. 49, 8174–8186. http://dx.doi.org/10.1002/2012WR012795.

Chen, S., Hong, Y., Cao, Q., Gourley, J.J., Tian, Y., Hardy, J., Kirstetter, P.E., Yong, B., Shen, Y., 2013b. Similarity and difference of the two successive V6 and V7 TRMM multisatellite precipitation analysis performance over China. J. Geophys. Res. 118, 13060–13074. http://dx.doi.org/10.1002/2013JD019964.

Ebert, E.E., 2007. Methods for Verifying Satellite Precipitation Estimates. Measuring Precipitation from Space - EURAINSAT and the future, Advances in Global Change Research 28 pp. 345–356.40.

Hong, Y., Gochis, D., Cheng, J., Hsu, K.-L., Sorooshian, S., 2007. Evaluation of PERSIANN-CCS Rainfall Measurement Using the NAME Event Rain Gauge Network. J. Hydrometeorol 8, 469–482. http://dx.doi.org/10.1175/JHM574.1.

Huffman, G.J., Bolvin, D.T., 2013. TRMM and Other Data Precipitation Data Set Documentation. Available online:, ftp://meso-a.gsfc.nasa.gov/pub/trmmdocs/3B42_3B43_doc.pdf (accessed on 29 April 2014).

Huffman, G.J., Adler, R.F., Rudolph, B., Schneider, U., Keehn, P., 1995. Global precipitation estimates based on a technique for combining satellite-based estimates, rain gauge analysis, and NWP model precipitation information. J. Clim. 8, 1284–1295.

Huffman, G.J., Adler, R.F., Morrissey, M., Bolvin, D.T., Curtis, S., Joyce, R., McGavock, B., Susskind, J., 2001. Global precipitation at one-degree daily resolution from multi-satellite observations. J. Hydrometeor. 2 (1), 36–50.

Huffman, G.J., Adler, R.F., Bolvin, D.T., Gu, G., Nelkin, E.J., Bowman, K.P., Hong, Y., Stocker, E.F., Wolff, D.B., 2007. The TRMM Multi-satellite Precipitation Analysis: Quasi-Global, Multi-Year, Combined-Sensor Precipitation Estimates at Fine Scale. J. Hydrometeorol. 8 (1), 38–55.

Huffman, G.J., Adler, R.F., Bolvin, D.T., Nelkin, E.J., 2010. The TRMM Multi-satellite Precipitation Analysis (TAMPA). In: Hossain, F., Gebremichael, M. (Eds.), Chapter 1 in Satellite Rainfall Applications for Surface Hydrology. Springer Verlag. ISBN: 978-90-481-2914-0, pp. 3–22.

Huffman, G.J., Adler, R.F., Bolvin, D.T., Nelkin, E.J., 2012. Global Precipitatiion in the GPCP Version 2.2, TMPA Version 7, and the Future. Available online:, https://www.bgs.ac.uk/changingwatercycle/downloads/July2012/Robust_Changes_Huffman_slides.pdf (last access: October 9, 2014).

Joyce, R.J., Janowiak, J.E., Arkin, P.A., Xie, P., 2004. CMORPH: A method that produces global precipitation estimates from passive microwave and infrared data at high spatial and temporal resolution. J. Hydrometeorol. 5, 487–503.

Liu, Z., Rui, H., Teng, W., Chiu, L, Leptoukh, G., Vicente, G., 2007. Online visualization and analysis: A new avenue to use satellite data for weather, climate and interdisciplinary research and applications. Measuring Precipitation from Space - EURAINSAT and the future, Advances in Global Change Research 28 pp. 549–558.

Liu, Z., Rui, H., Teng, W., Chiu, L.S., Leptoukh, G.G., Kempler, S., December 2009. 2009: Developing an Online Information System Prototype for Global Satellite Precipitation Algorithm Validation and Intercomparison. J. Appl. Meteorol. Climatol.-IPWG Spec. Issue 48 (12), 2581–2589.

Liu, Z., Ostrenga, D., Teng, W., Kempler, S., 2012. Tropical Rainfall Measuring Mission (TRMM) Precipitation Data and Services for Research and Applications. Bull. Am. Meteorol. Soc. http://dx.doi.org/10.1175/BAMS-D-11-00152.1.

Liu, Z., Ostrenga, D., Teng, W., Kempler, S., Milich, L., 2014. Developing GIOVANNI-based online prototypes to intercompare TRMM-related global gridded-precipitation products. Comput. Geosci. 66, 168–181.

Mahrooghy, M., Anantharaj, V.G., Younan, N.H., Aanstoos, J., Hsu, K.-L., 2012. On an Enhanced PERSIANN-CCS Algorithm for Precipitation Estimation. J. Atmos. Ocean. Technol. 29, 922–932. http://dx.doi.org/10.1175/JTECH-D-11-00146.1.

Prakash, S., Mahesh, C., Gairola, R.M., 2013. Comparison of TRMM Multi-satellite Precipitation Analysis (TMPA)-3B43 version 6 and 7 products with rain gauge data from ocean buoys. Remote Sens. Lett. 4 (7), 677–685.

Prakash, S., Mitra, A.K., Momin, I.M., Pai, D.S., Rajagopal, E.N., Basu, S., 2014. Comparison of TMPA-3B42 versions 6 and 7 Precipitation Products with Gauge based Data over India for the South-West Monsoon Period. J. Hydrometeorol. http://dx.doi.org/10.1175/JHM-D-14-0024.1 (e-View (early online release).

Qiao, L., Hong, Y., Chen, S., Zou, C.B., Gourley, J.J., Yong, B., 2014. Performance assessment of the successive Version 6 and Version 7 TMPA products over the climate-transitional zone in the southern Great Plains, USA. J. Hydrometeorol. 513, 446–456.

Sorooshian, S., Hsu, K.-L., Gao, X., Gupta, H.V., Imam, B., Braithwaite, D., 2000. Evaluation of PERSIANN System Satellite–Based Estimates of Tropical Rainfall. Bull. Am. Meteorol. Soc. 81, 2035–2046. http://dx.doi.org/10.1175/1520-0477(2000)081<2035:EOPSSE>2.3.CO;2.

Yong, B., Chen, B., Gourley, J.J., Ren, L., Hong, Y., Chen, X., Wang, W., Chen, S., Gong, L., 2014a. Intercomparison of the Version-6 and Version-7 TMPA precipitation products over high and low latitudes basins with independent gauge networks: Is the newer version better in both real-time and post-real-time analysis for water resources and hydrologic extremes? J. Hydrol. 508, 77–87. http://dx.doi.org/10.1016/j.jhydrol.2013.10.050.

Yong, B., Liu, D., Gourley, J.J., Tian, Y., Huffman, G.J., Ren, L., Hong, Y., 2014b. Global view of real-time TRMM Multi-satellite Precipitation Analysis: implication to its successor Global Precipitation Measurement mission. Bull. Am. Meteorol. Soc. http://dx.doi.org/10.1175/BAMS-D-14-00017.1 (e-View).

Zulkafli, Z., Buytaert, Wouter, Onof, Christian, Manz, Bastian, Tarnavsky, Elena, Lavado, Waldo, Guyot, Jean-Loup, 2014. A Comparative Performance Analysis of TRMM 3B42 (TMPA) Versions 6 and 7 for Hydrological Applications over Andean–Amazon River Basins. J. Hydrometeorol 15, 581–592. http://dx.doi.org/10.1175/JHM-D-13-094.1.